Applied Physics Letters

RESEARCH ARTICLE | JUNE 18 2026

Polarity effects on the growth of Si-doped AlGaN epilayers on AlN FREE

H. Alwan ; T. Njuguna ; D. Shima ; G. Balakrishnan ; J. Li ; J. Y. Lin ; H. X. Jiang

Appl. Phys. Lett. 128, 241907 (2026)
https://doi.org/10.1063/5.0331854

Polarity effects on the growth of Si-doped AlGaN epilayers on AlN

Cite as: Appl. Phys. Lett. **128**, 241907 (2026); doi: 10.1063/5.0331854
Submitted: 28 February 2026 · Accepted: 1 June 2026 ·
Published Online: 18 June 2026

View Online Export Citation CrossMark

H. Alwan,[1] T. Njuguna,[1] D. Shima,[2] G. Balakrishnan,[2] J. Li,[1] J. Y. Lin,[1] and H. X. Jiang[1,a)]

AFFILIATIONS

[1]Department of Electrical and Computer Engineering, Texas Tech University, Lubbock, Texas 79409, USA
[2]Center for High Technology Materials, University of New Mexico, Albuquerque, New Mexico 87106, USA

[a)]Author to whom correspondence should be addressed: hx.jiang@ttu.edu

ABSTRACT

We investigate the polarity dependent properties of Si-doped n-type AlGaN epilayers grown via metal organic chemical vapor deposition on Al- and N-polar AlN bulk substrates. While X-ray diffraction confirmed comparable crystalline quality for both polarities, photoluminescence spectroscopy revealed distinct optical signatures, suggesting varying levels of defect complexes involving aluminum vacancies and oxygen impurities. Electrical characterization via Hall-effect measurements showed a sharp contrast in transport properties. The N-polar epilayer exhibited a slight reduction in free electron concentration, but a significant decrease in electron mobility by over an order of magnitude compared to the Al-polar epilayer. Microstructural analysis through scanning transmission electron microscopy and energy-dispersive spectroscopy identified polarity-specific features at the AlGaN/AlN interface including increased lattice distortion and the presence of localized oxygen impurities in the N-polar samples, despite uniform Al and Ga distribution. These findings highlight substrate polarity as a key factor influencing the overall material quality and the performance of AlGaN-based devices, offering useful insights for optimizing n-type conductivity in polarity-engineered applications such as AlN and AlGaN-based vertical p-n diodes, vertical photoconductive semiconductor switch devices, and high electron mobility transistors.

AlGaN and AlN wide and ultra-wide bandgap semiconductors have attracted significant attention over the past decade due to their critical roles in deep-ultraviolet (DUV) optoelectronic and electronic applications.[1–5] These include photodetectors, light-emitting diodes and laser diodes, and high-power electronic devices. Because of their large direct energy bandgap translating to high critical field, high thermal conductivity, strong chemical stability, and excellent radiation hardness, AlGaN alloys with high Al-contents are especially suited for applications in high voltage/power/temperature environments.[6–8] The full miscibility of AlGaN alloys across the entire composition range enables continuous bandgap tuning from GaN to AlN.[9] This makes them versatile materials for DUV photonics and high-frequency electronics devices.[10] Despite these advantages, the performance of AlGaN-based devices is often limited by polarity dependent growth behavior, defect formation, and doping efficiency.[11–20] These issues are particularly severe in AlGaN alloys with high Al-compositions. Native point defects, such as aluminum and gallium vacancies and their complexes with oxygen and other impurities, introduce deep electronic states within the bandgap.[9,12–14,21–26] These defects adversely affect the carrier transport and optical properties. They act as carrier traps and scattering centers, reducing electron mobility, lowering conductivity, and degrading optical efficiency.[12–14,21–26] Understanding the origin and behavior of such defects is essential for further improving material quality and advancing device development.

Crystal polarity plays a critical role in governing surface kinetics, impurity incorporation, and defect formation in the epitaxial growth of III-nitride materials.[27] Al-polar and N-polar surfaces show fundamentally different adatom diffusion, bonding configurations, and incorporation pathways. This results in pronounced differences in structural, optical, and electrical properties. While polarity dependent growth behavior has been extensively studied in GaN, only a limited number of studies have explored polarity effects in high Al-content AlGaN epilayers grown on bulk AlN substrates, with prior works largely focused on heterostructure-based transport or device demonstrations.[18–20] A systematic comparison of material properties under identical growth conditions is still needed. Critically, the III-nitride community recognizes that achieving high crystalline quality AlGaN epilayers is significantly more challenging on N-polar than on Al-polar surfaces. The fundamental origins of this disparity remain poorly understood. Specifically, direct comparative studies of Si-doped, high Al-content AlGaN grown on Al- and N-polar bulk AlN substrates are scarce, as epitaxial growth has focused primarily on

Al-polar templates. In this work, we present a comparative study of n-type $Al_{0.4}Ga_{0.6}N$ epilayers grown on Al-polar and N-polar bulk AlN substrates. We focus on polarity dependent structural, optical, electrical, and microstructural properties. Through a combination of X-ray diffraction (XRD), photoluminescence (PL), Hall-effect measurements, electron microscopy, and compositional analysis, we elucidate how polarity fundamentally dictates the structural, optical, and electrical properties of Si-doped AlGaN.

Si-doped $Al_{0.4}Ga_{0.6}N$ epilayers were grown on 4-in. bulk AlN substrates with both Al-polar and N-polar orientations by metal organic chemical vapor deposition (MOCVD). Trimethylaluminum (TMAl), trimethylgallium (TMGa), and ammonia (NH_3) were used as the Al, Ga, and N precursors, respectively, with hydrogen serving as the carrier gas. For Si doping, silane (SiH_4) was transported into the reactor. The $Al_{0.4}Ga_{0.6}N$ epilayers were deposited with a thickness of approximately 0.3 μm under identical growth conditions on both Al-polar and N-polar substrates to enable a direct comparison of crystalline quality and surface morphology. The freestanding c-plane AlN bulk substrates with a thickness of approximately 600 μm were produced by Crystal IS by the physical vapor transport (PVT) method. Under the PVT growth conditions, Al stabilization on the top surface is a self-reinforcing kinetic process.[5,8] Prior to epitaxial growth, the substrates were treated by chemical mechanical polishing (CMP) processing using 0.2 μm colloidal SiO_2 and used without the deposition of any intermediate buffer layers with the aim to directly assess the polarity dependent growth behavior. The AlGaN epilayer preserves the polarity of the underlying AlN substrate surface. This is because wurtzite AlN and AlGaN share the same crystal structure, and the AlGaN epilayer tends to inherit the atomic stacking sequence and surface termination (polarity) of the AlN substrate during homoepitaxial growth. A Rigaku SmartLab X-ray diffractometer (with an angular resolution of about 100 arc sec) was utilized for XRD characterization to evaluate the structural properties of the epilayers. Room-temperature and 10 K PL emission spectroscopy were employed to probe the optical properties. The PL system consists of a frequency-quadrupled femtosecond (fs) Ti:sapphire laser ($\lambda_{exc} = 195$ nm, 6.35 eV) operating at 76 MHz with an average optical power of 1 mW, with a laser spot size of about 20 μm in diameter, providing an excitation power density of about 320 W/cm^2 and a 1.3 m monochromator in conjunction with a microchannel plate photomultiplier tube (MCP-PMT). Hall-effects measurements were performed to determine the carrier concentration, mobility, and resistivity of the samples. Microstructural and compositional analyses were performed using a JEOL NEOARM 200CF atomic resolution aberration corrected scanning transmission electron microscope (STEM/TEM), equipped with a cold field emission gun (FEG) and an ultrahigh-resolution pole piece. SEM and TEM modes were utilized to examine the surface features and cross-sectional microstructures of the AlGaN epilayers. Selected-area electron diffraction (SAED) patterns were collected to evaluate epitaxial alignment and crystalline quality. Elemental analysis was carried out using the integrated JEOL SDD 100 mm^2 energy-dispersive x-ray spectroscopy (EDS) detectors, supported by the Oxford Instruments Aztec software.

The schematic layer structures of the AlGaN epilayers are shown in Fig. 1(a), where (a1) and (a2) illustrate AlGaN epilayers grown on Al- and N-terminated AlN bulk substrates, respectively. Figure 1(b)

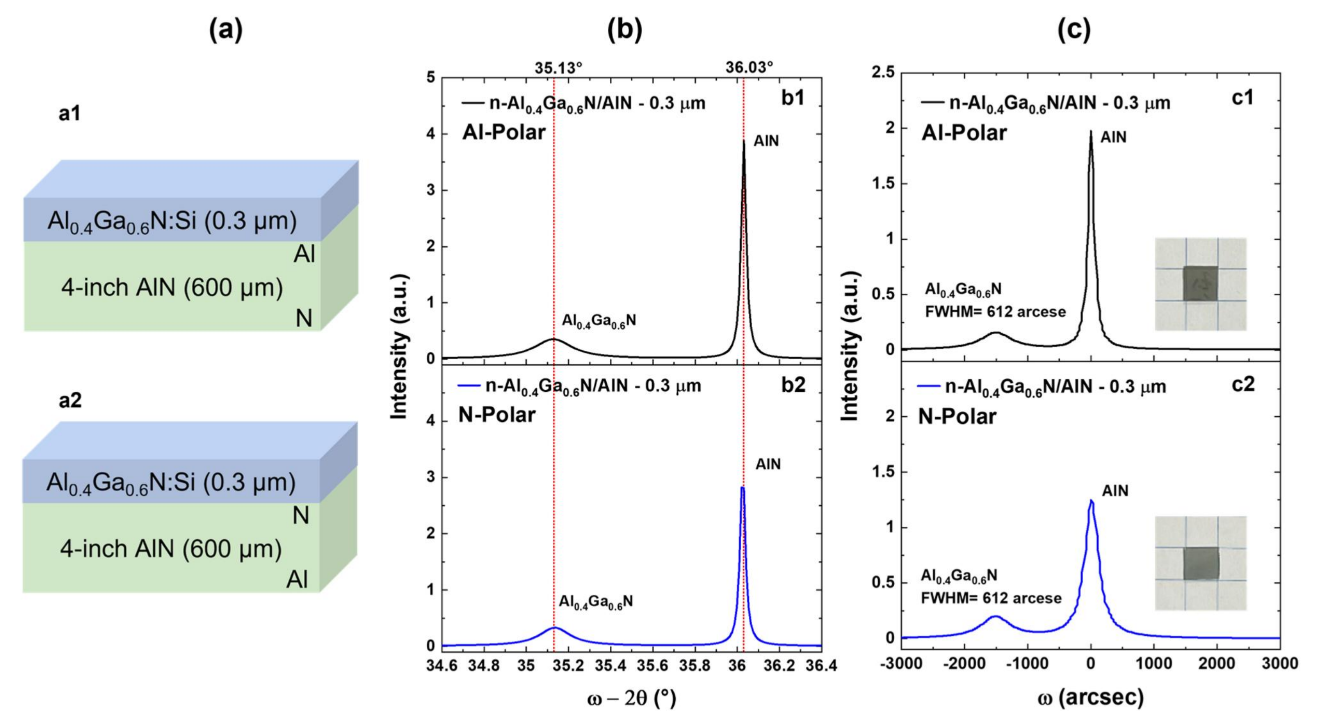

FIG. 1. (a) Schematic layer structures of AlGaN epilayers. X-ray diffraction spectra in (b) ω–2θ and (c) rocking-curve (ω) scans confirm the epitaxial growth of n-$Al_{0.4}Ga_{0.6}N$ on both Al-polar and N-polar of AlN bulk substrate. The optical images for the samples are also shown in the insets in (c).

compares the XRD spectra in ω–2θ scans covering the AlGaN (002) diffraction peak for epilayers grown on both Al-polar and N-polar substrates. The observed peak in both epilayers at $2\theta \sim 35.13°$ clearly separates from the AlN substrate peak at $\sim 36.03°$. This confirms a coherent epitaxial growth without the formation of secondary phases for both polarities. The Al composition in the $Al_xGa_{1-x}N$ epilayers estimated from the 2θ peak position using Vegard's law by a linear interpolation between AlN and GaN is about $x = 0.4$. The absence of peak splitting or asymmetrical behavior indicates a uniform alloy composition and well controlled strain within the (0.3 μm) AlGaN epilayers. Rocking-curve measurements (or ω-scans) were also utilized to probe crystal tilt and mosaicity of the AlGaN (002) peak, as shown in Fig. 1(c), yielding an identical full width at half maximum (FWHM) of approximately 612 arc sec for both Al-polar and N-polar samples, implying comparable mosaic spread and similar threading dislocation density.

Figure 2 shows the PL spectra of Si-doped $Al_{0.4}Ga_{0.6}N$ epilayers grown on Al-polar and N-polar AlN substrates measured at 300 and 10 K under 195 nm excitation. At room-temperature, as shown in Fig. 2(a), both samples exhibit a band edge emission around 4.23 eV, accompanied by sub-bandgap emission lines in the region of 2.7–2.9 eV (2.75 eV for the Al-polar sample and 2.89 eV for the N-polar sample) due to deep-level recombination processes. Similar defect-related emission features have been reported in high purity AlN and doped AlN epilayers, where Al-vacancy (V_{Al}) related defects dominate the sub-bandgap optical transitions.[28,29] In AlGaN, emission in this energy range has been widely associated with Al-vacancy-related defects, with moderate energy shifts compared to AlN due to alloy and bandgap bowing effects. A clear polarity-dependence is observed in the near-band edge region. The Al-polar sample exhibits a pronounced near-band edge emission at 4.23 eV, indicating that band edge recombination is the dominant radiative transition, whereas the N-polar sample shows a suppressed band edge emission at 4.23 eV with the defect-related transition near 2.89 eV being more dominant. The N-polar sample also exhibits an additional peak at 3.78 eV, which is related to the recombination of (V_{Al}-O_N)-related defect complexes. This interpretation is based on a previous experimental study, demonstrating that (V_{Al}-O_N) defect complexes in AlGaN introduce emission lines in the same energy range.[12] Consequently, the results shown in Fig. 2 imply a higher defect and impurity density in the N-polar epilayer.[24]

The low temperature (10 K) PL spectrum shown in Fig. 2(b) resolved two band edge emission lines in the Al-polar sample, including a strong emission line at $\sim$4.21 eV, attributed to the excitonic recombination and another weaker emission line at a higher energy position near 4.30 eV, most likely associated with the band-to-band recombination. In contrast, the excitonic emission peak near 4.21 eV is absent in the N-polar sample. Instead, it exhibits multiple peaks at approximately 2.89, 3.78, and 4.30 eV, confirming that defect-assisted recombination dominates, with weaker band edge contributions in comparison to the Al-polarity epilayer. Although the epilayers are Si-doped, a distinct Si-related recombination peak was not resolved. This is likely because the localization energy of the excitons is comparable to the donor binding energy of Si in AlGaN alloys,[22,30] resulting in significant spectral overlap between localized excitonic transitions and Si donor-related emission. Overall, the PL results indicate that the band edge transitions dominate in the Al-polar epilayer, while defect-related recombination lines dominate in the N-polar epilayer, highlighting the critical role of substrate polarity in defect formation and optical recombination mechanisms in Si-doped AlGaN epilayers.

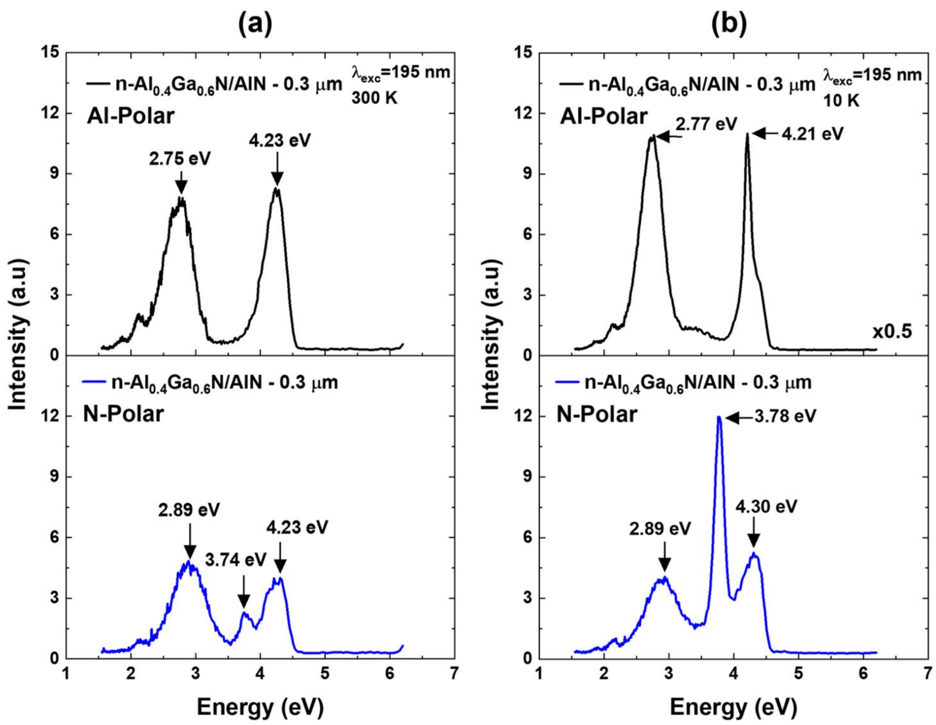

FIG. 2. (a) Room-temperature (T = 300 K) and (b) low temperature (T = 10 K) photoluminescence spectra excited by a fs laser (λ_{exc} = 195 nm) of n-$Al_{0.4}Ga_{0.6}N$ epilayers grown on Al-polar and N-polar AlN substrates.

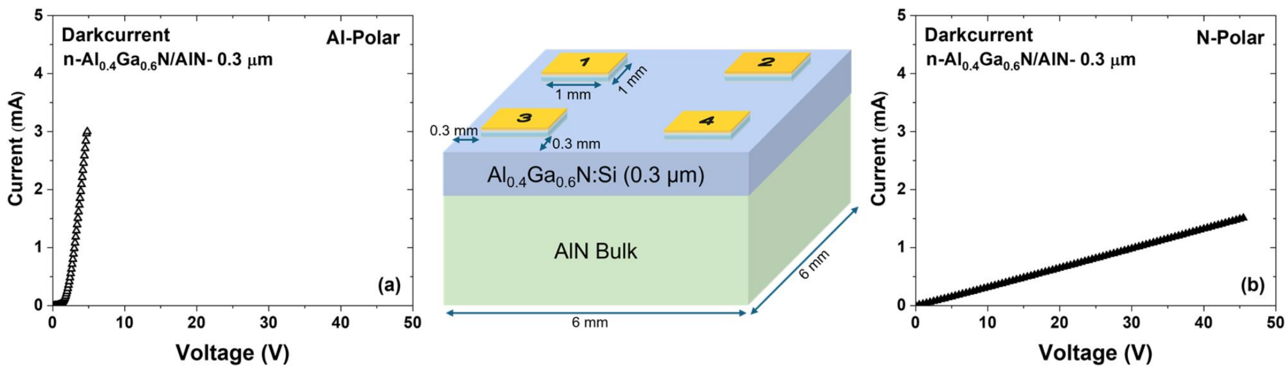

FIG. 3. Current voltage (I–V) characteristics of n-AlGaN epilayers grown on bulk AlN substrates with (a) Al-polar and (b) N-polar orientations, probed between contacts 1 and 2. The inset shows the schematic of van der Pauw samples fabricated for I–V characteristics and Hall-effect measurements.

To characterize and compare the electrical properties of n-AlGaN epilayers deposited on Al- and N-polar substrates, van der Pauw samples were fabricated. As schematically shown in the inset of Fig. 3, ohmic contacts consisting of Ti (15 nm)/Al (10 nm)/Ti (20 nm)/Au (35 nm) layers were deposited on the four corners of the samples using e-beam evaporation via identical masks followed by rapid thermal annealing in N_2 at 900 °C for 2 min. Current voltage (I–V) characteristics between contacts 1 and 2 were measured and compared for both samples. In comparison, the Al-polar sample exhibits a markedly higher current than the N-polar sample. This behavior suggests reductions in the free electron concentration and mobility due to enhanced carrier scattering and compensation in the N-polar epilayer.

To further assess the influence of substrate polarity on charge transport and to minimize the contributions of contacts to the measurement results, Hall-effect studies were conducted using van der Pauw samples. Table I summarizes the room-temperature electrical properties of Si-doped AlGaN epilayers grown on Al-polar and N-polar AlN substrates, probed by Hall-effect measurements. A pronounced polarity dependence is observed in all electrical parameters. The Al-polar sample exhibits a relatively high electron mobility of 33.4 cm^2/V s, which is more than an order of magnitude larger than a value of 1.24 cm^2/V s for the N-polar sample. Nevertheless, the exact mechanism underlying the mobility reduction warrants further investigation, and temperature-dependent Hall-effect measurements could provide valuable insights. The significant difference observed between Al- vs N-polar AlGaN alloys in terms of electron mobility corroborates the PL results of Fig. 2 and again indicates the presence of higher numbers of defects and impurities in N-polar AlGaN. Correspondingly, the Al-polar epilayer possesses a much lower resistivity of 0.012 Ω cm compared to 0.55 Ω cm for the N-polar sample. The electron concentrations of the two samples are of the same order of magnitude, with $n = 1.50 \times 10^{19}\ cm^{-3}$ for the Al-polar sample and $n = 0.91 \times 10^{19}\ cm^{-3}$ for the N-polar sample, indicating that the large difference in resistivity is primarily governed by the carrier mobility rather than the carrier concentration. The significantly reduced mobility in the N-polar epilayer suggests enhanced carrier scattering and compensation effects, likely arising from higher densities of defect and impurity related complexes. This interpretation is consistent with the PL results, which reveal stronger defect-related emissions in the N-polar sample due to enhanced defect-assisted non-radiative and radiative recombination pathways. The lower electron concentration observed in the N-polar sample further supports the presence of enhanced carrier compensation and reduced free-carrier transport efficiency.

TABLE I. Electrical properties probed by Hall-effect measurements (electron mobility, electron concentration, resistivity, and Hall coefficient) of Si-doped AlGaN epilayers grown on Al-polar and N-polar AlN substrates.

Parameter	Al-polar	N-polar
Electron mobility (cm^2/V s)	33.4 ± 2.1	1.24 ± 0.08
Carrier concentration ($\times 10^{19}\ cm^{-3}$)	1.50 ± 0.06	0.91 ± 0.19
Resistivity (Ω cm)	0.012 ± 0.001	0.55 ± 0.11

Figures 4(a) and 4(b) show the cross-sectional STEM images of n-AlGaN epilayers grown on Al-polar and N-polar AlN substrates, respectively. Both samples exhibit an abrupt and coherent AlGaN/AlN interface with continuous lattice fringes across the heterointerface, confirming high-quality epitaxial growth without interfacial amorphous layers or secondary phases. The Al-polar sample shows uniform lattice contrast throughout the AlGaN layer, whereas the N-polar sample exhibits slightly enhanced contrast variations, which may be associated with local strain fluctuations or increased point-defect-related disorder. These observations are consistent with the polarity dependent optical and electrical characteristics discussed earlier.

Figure 5(a) shows the SAED patterns obtained from the AlN substrate (a1) and the overgrown n-AlGaN epilayer of the Al-polar orientation (a2). The diffraction spots from the n-AlGaN epilayer are relatively uniform and nearly circular, indicating good crystallographic ordering and minimal in-plane lattice distortion. In addition, the reduced reciprocal space spacing of the n-AlGaN reflections compared to AlN is consistent with a larger real space lattice constant of the AlGaN alloy. In contrast, the SAED patterns of the N-polar epilayer sample shown in Fig. 5 reveal noticeably broadened and elongated diffraction spots in the n-AlGaN layer. Such spot spreading indicates increased lattice distortion and local rotational disorder, suggesting a higher degree of strain relaxation and defect-related disorder under N-polar growth conditions. The smaller reciprocal space spacing of the AlGaN reflections again indicates the larger lattice constant

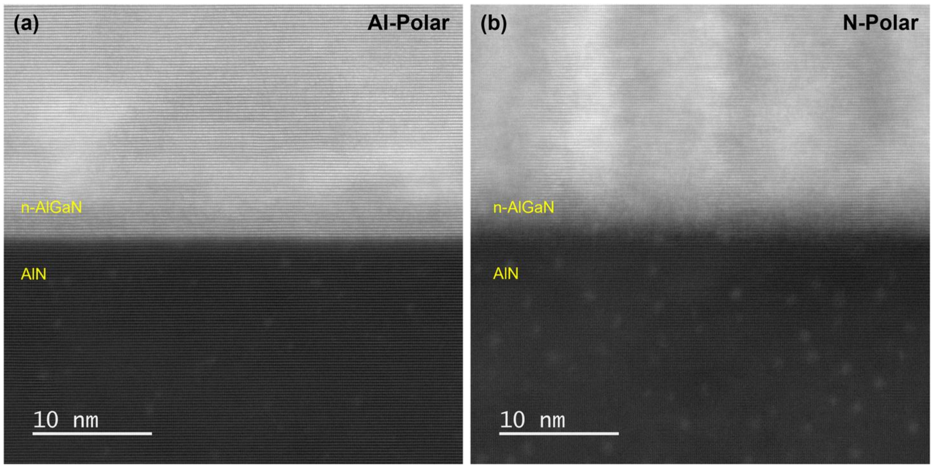

FIG. 4. Cross-sectional STEM images of n-AlGaN epilayers grown on bulk AlN substrates with (a) Al-polar and (b) N-polar orientations.

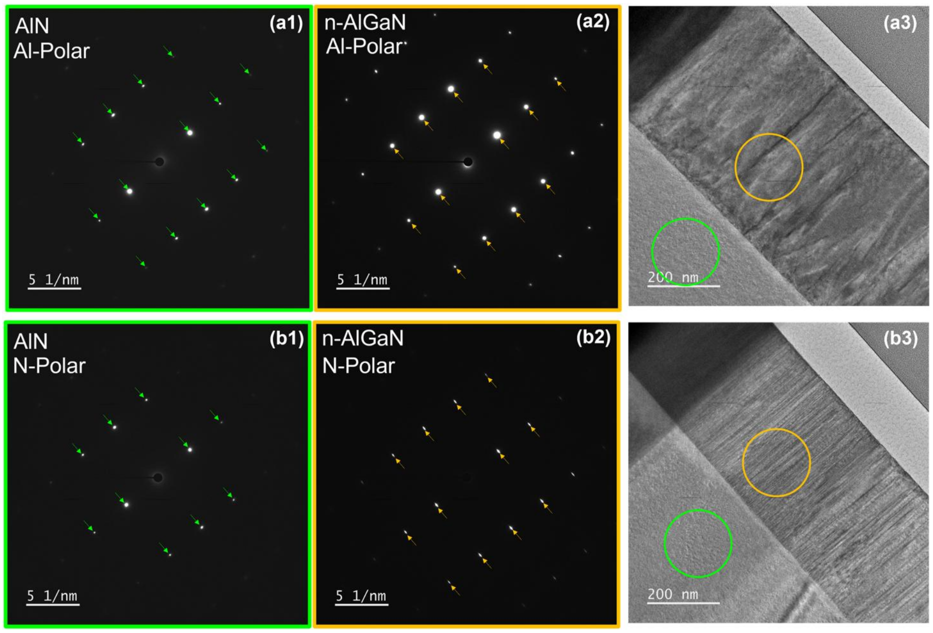

FIG. 5. Selected-area electron diffraction patterns and corresponding STEM images acquired from the AlN substrate and the n-AlGaN epilayers for (a) Al-polar and (b) N-polar heterostructures.

of the AlGaN layer relative to AlN. Overall, the SAED results confirm coherent epitaxial alignment for both polarities while revealing increased lattice distortion in the N-polar n-AlGaN epilayer.

Figure 6(a) shows the EDS line-scan profile across the Al-polar n-AlGaN/AlN interface. A sharp transition in Al and Ga concentrations is observed at the heterointerface, indicating an abrupt compositional change and uniform alloy composition within the n-AlGaN layer. The oxygen and carbon signals remain low and relatively constant across the scan, suggesting minimal impurity incorporation and a chemically abrupt interface. In contrast, the N-polar sample shown in Fig. 6(b) exhibits a noticeable enhancement of the oxygen signal localized near the n-AlGaN/AlN interface, as highlighted by the yellow circle. This localized oxygen enrichment, accompanied by a more gradual compositional transition, suggests increased interfacial impurity incorporation under N-polar growth conditions. Such behavior is consistent with reports on N-polar GaN and AlGaN epilayers, where N-face growth is known to promote enhanced impurity incorporation and interfacial nonstoichiometry due to distinct surface bonding configurations and growth kinetics.[12–14]

In summary, Si-doped $Al_{0.4}Ga_{0.6}N$ epilayers were grown on Al-polar and N-polar bulk AlN substrates under identical MOCVD conditions to examine polarity dependent growth behavior. Structural characterization confirms coherent epitaxial growth for both polarities, while optical and electrical measurements reveal pronounced polarity driven differences. The Al-polar epilayer exhibits strong near-band edge emission and superior electron transport, whereas the N-polar epilayer shows stronger defect-related luminescence and reduced carrier mobility, consistent with polarity dependent impurity incorporation and defect formation previously reported in N-polar GaN and AlGaN systems. These results establish substrate polarity as a key

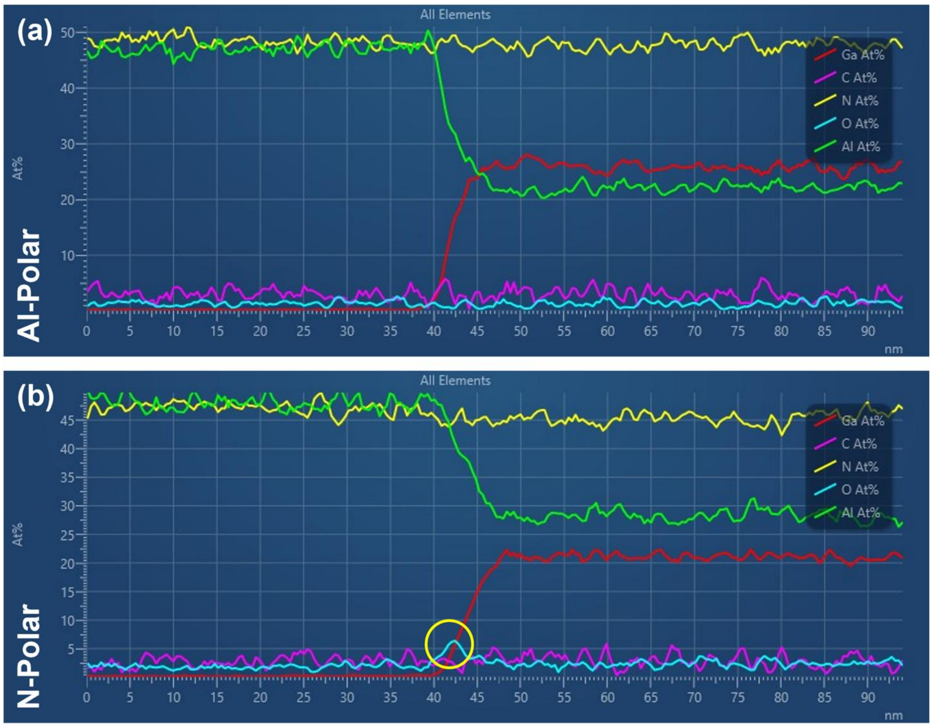

FIG. 6. EDS line-scan profiles across the n-AlGaN/AlN interface for (a) Al-polar and (b) N-polar samples, showing the atomic percentages of Al, Ga, N, O, and C as a function of depth.

parameter governing defect formation, optical recombination, and charge transport in AlGaN epilayers, providing a more complete experimental framework for polarity-controlled growth of AlGaN epilayers.

The information, data, or work presented herein was funded in part by the Advanced Research Projects Agency-Energy (ARPA-E), U.S. Department of Energy, under ULTRAFAST program, Award No. DE-AR0001821, monitored by Dr. Johan Enslin, Dr. Olga Spahn, and Dr. Eric Carlson. Electron microscopy was carried out in the Nanomaterials Characterization Facility at the University of New Mexico, a facility that is supported by the State of New Mexico, the National Science Foundation, and the National Aeronautics and Space Administration. The acquisition of the JEOL NEOARM AC-S/TEM at the University of New Mexico was supported by NSF under Grant No. DMR-1828731 and NASA Emerging Worlds under Grant No. 80NSSC21K1757. The views and opinions of authors expressed herein do not necessarily state or reflect those of the United States Government or any agency thereof. Jiang and Lin are grateful to the AT&T Foundation for the support of Ed Whitacre and Linda Whitacre endowed chairs.

AUTHOR DECLARATIONS

Conflict of Interest

The authors have no conflicts to disclose.

Author Contributions

H. Alwan: Data curation (equal); Formal analysis (equal); Investigation (equal); Methodology (equal); Software (equal); Validation (equal); Visualization (equal); Writing – original draft (equal). **T. Njuguna:** Data curation (equal); Formal analysis (equal); Investigation (equal); Methodology (equal); Software (equal); Validation (equal); Visualization (equal). **D. Shima:** Data curation (equal); Formal analysis (equal); Investigation (equal); Methodology (equal); Software (equal); Validation (equal); Visualization (equal); Writing – review & editing (equal). **G. Balakrishnan:** Data curation (equal); Formal analysis (equal); Investigation (equal); Methodology (equal); Software (equal); Validation (equal); Visualization (equal); Writing – review & editing (equal). **J. Li:** Data curation (equal); Formal analysis (equal); Investigation (equal); Methodology (equal); Project administration (equal); Resources (equal); Software (equal); Supervision (equal); Validation (equal); Visualization (equal). **J. Y. Lin:** Conceptualization (equal); Formal analysis (equal); Funding acquisition (equal); Investigation (equal); Methodology (equal); Project administration (equal); Resources (equal); Supervision (equal); Validation (equal); Visualization (equal); Writing – original draft (equal); Writing – review & editing (equal). **H. X. Jiang:** Conceptualization (equal); Formal analysis (equal); Funding acquisition (equal); Investigation (equal); Methodology (equal); Project administration (equal); Resources (equal); Supervision (equal); Validation (equal); Visualization (equal); Writing – original draft (equal); Writing – review & editing (equal).

DATA AVAILABILITY

The data that support the findings of this study are available within the article.

REFERENCES

[1]H. X. Jiang and J. Y. Lin, "AlN epitaxial layers for UV photonics," in *Optoelectronic Devices: III-Nitride*, edited by M. Razeghi and M. Heini (Elsevier Ltd., 2004), Chap. 7.

[2]M. A. Khan, K. Balakrishnan, and T. Katona, "Ultraviolet light-emitting diodes based on group three nitrides," Nat. Photonics **2**, 77 (2008).
[3]C. Pernot, M. Kim, S. Fukahori, T. Inazu, T. Fujita, Y. Nagasawa, A. Hirano, M. Ippommatsu, M. Iwaya, S. Kamiyama, I. Akasaki, and H. Amano, "Improved efficiency of 255–280 nm AlGaN-based light-emitting diodes," Appl. Phys. Express **3**, 061004 (2010).
[4]M. Kneissl, Z. Yang, M. Teepe, C. Knollenberg, O. Schmidt, P. Kiesel, N. M. Johnson, S. Schujman, and L. J. Schowalter, "Ultraviolet semiconductor laser diodes on bulk AlN," J. Appl. Phys. **101**, 123103 (2007).
[5]R. T. Bondokov, S. G. Mueller, K. E. Morgan, G. A. Slack, S. Schujman, M. C. Wood, J. A. Smart, and L. J. Schowalter, "Large-area AlN substrates for electronic applications: An industrial perspective," J. Cryst. Growth **310**, 4020 (2008).
[6]I. Prozheev, F. Mehnke, T. Wernicke, M. Kneissl, and F. Tuomisto, "Electrical compensation and cation vacancies in Al rich Si-doped AlGaN," Appl. Phys. Lett. **117**, 142103 (2020).
[7]R., Gaska, C., Chen, J., Yang, E., Kuokstis, A., Khan, G., Tamulaitis, I., Yilmaz, M. S., Shur, J. C., Rojo, and L. J., Schowalter, "Deep-ultraviolet emission of AlGaN/AlN quantum wells on bulk AlN," Appl. Phys. Lett. **81**, 4658 (2002).
[8]W. Li, Q. Liu, J. Tan, G. He, B. Li, Z. Sun, and H. Wu, "Recent advances in PVT growth of large-diameter, high-quality aluminum nitride single crystals," Cryst. Res. Technol. **60**(7), 2500038 (2025).
[9]K. B. Nam, M. L. Nakarmi, J. Y. Lin, and H. X. Jiang, "Deep impurity transitions involving cation vacancies and complexes in AlGaN alloys," Appl. Phys. Lett. **86**, 222108 (2005).
[10]W. A. Doolittle, C. M. Matthews, H. Ahmad, K. Motoki, S. Lee, A. Ghosh, E. N. Marshall, A. L. Tang, P. Manocha, and P. D. Yoder, "Prospectives for AlN electronics and optoelectronics and the important role of alternative synthesis," Appl. Phys. Lett. **123**, 070501 (2023).
[11]E. S. Hellman, "The polarity of GaN: A critical review," Mater. Res. Soc. Int. J. Nitride Semicond. Res. **3**, e11 (1998).
[12]F. Tuomisto, K. Saarinen, B. Lucznik, I. Grzegory, H. Teisseyre, T. Suski, S. Porowski, P. R. Hageman, and J. Likonen, "Effect of growth polarity on vacancy defect and impurity incorporation in dislocation-free GaN," Appl. Phys. Lett. **86**, 031915 (2005).
[13]D. F. Storm, D. S. Katzer, D. J. Meyer, and S. C. Binari, "Oxygen incorporation in homoepitaxial N-polar GaN grown by radio frequency-plasma assisted molecular beam epitaxy: Mitigation and modeling," J. Appl. Phys. **112**, 013507 (2012).
[14]C. Li, K. Zhang, Q. Zeng, X. Yin, X. Ge, J. Wang, and Z. Chen, "High quality N-polar GaN films grown with varied V/III ratios by metal−organic vapor phase epitaxy," RSC Adv. **10**, 43187 (2020).
[15]P. Wang, D. Wang, S. Mondal, Y. Wu, T. Ma, and Z. Mi, "Interfacial modulated lattice-polarity-controlled epitaxy of III-nitride heterostructures on Si (111)," ACS Appl. Mater. Interfaces **14**, 15747 (2022).
[16]S. Mondal, D. Wang, A. Uddin Bhuiyan, M. Hu, M. Reddeppa, P. Wang, H. Zhao, and Z. Mi, "Tunable bandgap and Si-doping in N-polar AlGaN on C-face 4H-SiC via molecular beam epitaxy," Appl. Phys. Lett. **123**, 182106 (2023).
[17]G. Namikawa, K. Shojiki, R. Yoshida, R. Kusuda, K. Uesugi, and H. Miyake, "MOVPE growth of AlN and AlGaN films on N-polar annealed and sputtered AlN templates," J. Cryst. Growth **617**, 127256 (2023).
[18]E. Kim, Z. Zhang, J. Singhal, K. Nomoto, A. Hickman, M. Toita, D. Jena, and H. G. Xing, "First demonstration of N-polar GaN/AlGaN/AlN HEMT on single crystal AlN substrates," in *Device Research Conference (DRC)* (IEEE, 2022).
[19]M. Noshin, X. Wen, R. Soman, X. Xu, and S. Chowdhury, "Growth and mobility characterization of N-polar AlGaN channel high electron mobility transistors," Appl. Phys. Lett. **123**, 062103 (2023).
[20]Y. H. Chen, J. Encomendero, C. Savant, V. Protasenko, H. G. Xing, and D. Jena, "Electron mobility enhancement by electric field engineering of AlN/GaN/AlN quantum-well HEMTs on single-crystal AlN substrates," Appl. Phys. Lett. **124**(15), 152111 (2024).
[21]C. G. Van de Walle and J. Neugebauer, "First-principles calculations for defects and impurities: Applications to III-nitrides," J. Appl. Phys. **95**, 3851 (2004).
[22]M. L. Nakarmi, K. H. Kim, K. Zhu, J. Y. Lin, and H. X. Jiang, "Transport properties of highly conductive n-type Al-rich $Al_xGa_{1-x}N$ ($x \geq 0.7$)," Appl. Phys. Lett. **85**, 3769 (2004).
[23]N. Nepal, M. L. Nakarmi, J. Y. Lin, and H. X. Jiang, "Photoluminescence studies of impurity transitions in AlGaN alloys," Appl. Phys. Lett. **89**, 092107 (2006).
[24]A. Sedhain, J. Y. Lin, and H. X. Jiang, "Nature of optical transitions involving cation vacancies and complexes in AlN and AlGaN," Appl. Phys. Lett. **100**, 221107 (2012).
[25]J. B. Varley, A. Janotti, and C. G. Van de Walle, "Defects in AlN as candidates for solid-state qubits," Phys. Rev. B **93**, 161201 (2016).
[26]S. F. Chichibu, A. Uedono, K. Kojima, H. Ikeda, K. Fujito, S. Takashima, M. Edo, K. Ueno, and S. Ishibashi, "The origins and properties of intrinsic nonradiative recombination centers in wide bandgap GaN and AlGaN," J. Appl. Phys. **123**, 161413 (2018).
[27]J. Speck and S. Chichibu, "Nonpolar and semipolar group III nitride-based materials," MRS Bull. **34**, 304 (2009).
[28]H. Alwan, M. Almohammad, J. Li, J. Y. Lin, and H. X. Jiang, "Optical properties of Zr-doped AlN epilayers," APL Mater. **13**, 071115 (2025).
[29]T. Njuguna, H. Alwan, K. Hogan, J. Grandusky, J. Li, J. Y. Lin, and H. X. Jiang, "Structural and optical properties of 100-mm AlN bulk single crystals," Appl. Phys. Lett. **127**, 182102 (2025).
[30]N. Nepal, J. Li, M. L. Nakarmi, J. Y. Lin, and H. X. Jiang, "Exciton localization in AlGaN alloys," Appl. Phys. Lett. **88**, 062103 (2006).